Appl Microbiol Biotechnol (2004) 63:407–417
DOI 10.1007/s00253-003-1357-9

ORIGINAL PAPER

K. Al Zaid Siddiquee · M. J. Arauzo-Bravo · K. Shimizu

Metabolic flux analysis of *pykF* gene knockout *Escherichia coli* based on ^{13}C-labeling experiments together with measurements of enzyme activities and intracellular metabolite concentrations

Received: 28 February 2003 / Revised: 19 April 2003 / Accepted: 25 April 2003 / Published online: 12 June 2003

Abstract Metabolic flux analysis based on ^{13}C-labeling experiments followed by the measurement of intracellular isotope distribution using both 2D NMR and GC-MS was carried out to investigate the effect of pyruvate kinase (*pyk*) gene knockout on the metabolism of *Escherichia coli* in continuous culture. In addition, the activities of 16 enzymes, and the concentrations of 5 intracellular metabolites, were measured as a function of time in batch culture as well as continuous culture. It was found that flux through phosphoenol pyruvate carboxylase and malic enzyme were up-regulated in the *pykF*$^-$ mutant as compared with the wild type, and acetate formation was significantly reduced in the mutant. In addition, flux through the phosphofructose kinase pathway was reduced and that through the oxidative pentose phosphate (PP) pathway increased in the mutant. This was evidenced by the corresponding enzyme activities, and the increase in the concentrations of phosphoenol pyruvate, glucose-6-phosphate and 6-phosphogluconate, etc. It was also found for continuous cultivation that the enzyme activities of the oxidative PP and Entner-Doudoroff pathways increased as the dilution rate increased for the *pykF*$^-$ mutant. To clarify the metabolism quantitatively, it was found to be quite important to integrate the information on intracellular metabolic flux distribution, enzyme activities and intracellular metabolite concentrations.

K. Al Zaid Siddiquee · M. J. Arauzo-Bravo · K. Shimizu (✉)
Department of Biochemical Engineering and Science,
Kyushu Institute of Technology,
Iizuka, 820–8502 Fukuoka, Japan
e-mail: shimi@bse.kyutech.ac.jp
Tel.: +81-948-297817
Fax: +81-948-297801

K. Shimizu
Institute for Advanced Biosciences,
Keio University,
Tsuroka, 997–0017 Yamagata, Japan

Introduction

A wealth of information is available on the genetic regulation, biochemistry and physiology of cellular metabolism, but surprisingly little is known about what controls the overall rate of substrate catabolism and metabolic flux distribution (Fraenkel 1992). The central metabolic pathway has both anabolic and catabolic functions, providing cofactors and building blocks for macromolecular synthesis as well as energy production. While some single-gene knockout mutations in central metabolism preclude growth on glucose, the majority can potentially be compensated for either using alternative enzymes or by re-routing carbon flux through alternative pathways. The phenotype of knock-out mutants is usually characterized by quantitative physiological analysis, with conclusions on intracellular metabolism then being drawn based on quantitative interpretation of these results.

Changes in cellular physiology, such as redirection of intermediary metabolism in response to a specific gene knock-out, and/or changes in culture conditions may affect metabolism (Tao et al. 1999). Many of these metabolic adjustments are accompanied by changes in metabolite concentrations and enzyme activities as well as metabolic flux distribution. In the present study, we investigated the effect of pyruvate kinase (*pyk*) gene knock-out on metabolism.

Pyruvate (PYR) is a key intermediate in catabolic and biosynthetic reactions, explaining why there are several metabolic routes that can deliver this compound. One of the major ways to synthesize PYR is through the activation of Pyk, which catalyzes the conversion of phosphoenol pyruvate (PEP) and ADP to produced PYR and ATP at the final stage of the glycolytic pathway. The resulting PYR is the first non-phosphorylated intermediate in the glycolytic pathway and plays a central role in metabolism (Ponce et al. 1995; Steiner et al. 1998). In *Escherichia coli*, there are two *pyk* isoenzymes, PykA and PykF, encoded by the *pykA* and *pykF* genes, respectively. It is known that *pykA* contributes little to *Pyk* activity.

Hence, in the present study, we investigated the effect of *pykF* gene knock-out on central metabolism.

To reveal cause and effect relationships, however, it is important to gain deeper insight into the complex metabolic responses at the level of intracellular metabolite concentrations and fluxes (Emmerling et al. 2002). For metabolic flux calculation, ^{13}C-labeling experiments with subsequent measurement of intracellular isotope distribution using NMR and/or GC-MS are required. In the present study, we combined 2-D NMR tracer data, which is based on the measurement of ^{13}C–^{13}C scalar coupling fine structures in the cellular amino acids, with mass isotopomer analysis, which separates and identifies isotopomers with different molecular/fragment mass. This combination improves the accuracy of determining metabolic flux distribution, but necessitates a more complicated algorithm to incorporate tracer data obtained from different sources into the metabolic model. The other useful method for metabolic analysis is to measure enzyme activities. It should be mentioned that intracellular carbon fluxes cannot usually be inferred directly from the enzyme activities, although the existence of the corresponding pathways may be inferred.

In the present investigation, we measured enzyme activities and intracellular metabolite concentrations as a function of time for both the *pykF*$^-$ mutant and wild type *E. coli* in batch culture to observe the dynamic characteristics of metabolism. Moreover, we carried out metabolic flux analysis based on ^{13}C-labeling experiments together with measurements of enzyme activities and intracellular metabolite concentrations in continuous culture to clarify quantitatively the effect of *pykF*$^-$ knock-out on metabolism.

Materials and methods

Strains and cultivation conditions

The strains used were wild type *E. coli* K-12 and the PykF (*pykF*$^-$) knockout mutant JWK1666, which was constructed by deletion of the corresponding gene *pykF* from *E. coli* derivative BW 25113 using the method of Datsenko and Wanner (2000) (see Mori et al. http://www.ttck.keio.ac.jp/IAB/english/research/index.htm).

For batch culture, a minimal medium consisting of 10 g glucose per liter, 48 mM Na_2HPO_4, 22 mM KH_2PO_4, 10 mM NaCl, and 40 mM $(NH_4)SO_4$, was used. For minimal medium, the following components were filter-sterilized separately and then added (per liter of final volume): 1 ml 1 M $MgSO_4$, 1 ml 0.1 mM $CaCl_2$, 1 ml vitamin B_1 (1 mg/l stock) and 10 ml trace element solution containing (per liter): 0.55 g $CaCl_2$, 1 g $FeCl_3$, 0.1 g $MnCl_2{\cdot}4H_2O$, 0.17 g $ZnCl_2$, 0.043 g $CuCl_2{\cdot}2H_2O$, 0.06 g $CoCl_2{\cdot}2H_2O$, and 0.06 g $Na_2MoO_4{\cdot}2H_2O$. Batch culture was conducted at 37°C in a working volume of 1 l in a 2 l reactor (M-100; Rikakiki, Tokyo, Japan) equipped with pH, dissolved oxygen and temperature sensors. The airflow was maintained at 1 l min^{-1}, and the dissolved oxygen concentration was kept at 3–4 ppm. The pH of the culture was maintained at 7.0 by automatic addition of 2.0 M HCl or 2.0 M NaOH with a pH controller. Continuous cultivation was conducted in a working volume of 500 ml in a 1 l reactor (Marubishi, Tokyo, Japan). The minimal medium used for continuous cultivation had the same composition as that for batch culture except that the feed glucose concentration was 5 g/l. The dilution rate (D) was either 0.1 h^{-1} or 0.5 h^{-1}, and the working volume was kept constant by removal of effluent by use of pre-calibrated peristaltic pumps.

Measurements of biomass and extracellular metabolite concentrations

Cell concentration was determined by measuring the optical density (OD) of the culture using a spectrophotometer (Ubet-30, Jasco, Tokyo, Japan), and then converted to dry cell weight (DCW) per liter based on the relationship between OD and DCW previously obtained. Glucose concentration was measured using an enzymatic kit (Wako, Osaka, Japan). Acetic acid and lactic acid concentrations were also measured using enzymatic kits (Boehringer, Mannheim, Germany). Oxygen and carbon dioxide concentrations in the bioreactor off-gas were measured using an off-gas analyzer (LX-750, Iijima Electronics, Japan).

Preparation of cell-free extract and enzyme assay

Samples were taken every 2 h during batch cultivation, while for continuous culture, samples were taken after the culture reached steady state. Cells were harvested by centrifugation at 10,000 *g* for 10 min, washed twice with 100 mM Tris-HCl (pH 7.0) containing 20 mM KCl, 5 mM $MnSO_4$, 2 mM DTT and 0.1 mM EDTA, and then resuspended in the same buffer (ca. 15 g wet weight cells in 50 ml buffer solution). Cells were disrupted by ten sonication steps in the ultrasonic disrupter (UD-201; Tomy, Tokyo, Japan) with 30-s intervals between each step. Cell debris was removed by centrifugation, and the resulting crude cell extracts were used immediately for determination of enzyme activity or stored at −20°C. All operations were carried out on ice.

Enzyme activities were measured spectrophotometrically under thermostatically controlled conditions (30°C) using a U-2000A spectrophotometer (Hitachi, Japan). All compounds of the reaction mixtures were pipetted into a cuvette with a 1-cm light path and reactions initiated by adding the cell extract or substrate to give a final volume of 1 ml. The wavelength and the millimolar extinction coefficients for NAD^+, NADH, $NADP^+$ and NADPH were 340 nm and 6.22 cm^{-1} mM^{-1}, respectively. One unit (U) of specific enzyme activity was defined as the amount of enzyme required to convert 1 μmol substrate into the specific product per minute per milligram of protein. Each measurement was performed in triplicate.

Assay conditions were as follows: Hexokinase (HXK): 0.1 M Tris-HCl (pH 7.5), 60 mM $MgCl_2$, 1 mM DTT, 0.5 mM $NADP^+$, 2 mM ATP, 15 mM glucose, 2 U glucose-6-phosphate dehydrogenase (G6PDH; Samuelov et al. 1991). Phosphofructokinase (PFK): 50 mM imidazole-HCl (pH 7.0), 0.1 M KCl, 10 mM $MgCl_2$, 1 mM EDTA, 0.25 mM NADH, 0.25 mM fructose-6-phosphate (F6P), 0.5 U aldolase, 0.5 U glycerolphosphate dehydrogenase, 0.5 U triosephosphate isomerase (TPI) (Gancedo and Gancedo 1971). Phosphoglucose isomerase (PGI): 0.1 M Tris-HCl (pH 7.8), 10 mM $MgCl_2$, 0.5 mM $NADP^+$, 1 U G6PDH, 2 mM F6P (Salas et al. 1965). TPI: 300 mM triethanolamine buffer (pH 7.8), 0.2 mM NADH, 1 U glycerol phosphate dehydrogenase, 5 mM glyceraldehyde-3-phosphate (GAP). PYK: 0.1 M Tris-HCl (pH 7.5), 5 mM ADP, 1 mM DTT, 10 mM KCl, 15 mM $MgCl_2$ 0.5 mM PEP, 0.25 mM NADH, 10 U lactate dehydrogenase (LDH; Sridhar et al. 2000). PEP carboxykinase (PCK): 0.1 M TES buffer (pH 6.6), 10 mM $MgCl_2$, 5 mM $MnCl_2$, 1 mM DTT, 10 mM ADP, 75 mM $NaHCO_3$, 0.3 mM NADH, 20 U malate dehydrogenase (MDH), 10 mM PEP (Van der Werf et al. 1997). PEP carboxylase (PPC): 66 mM Tris-HCl (pH 9.0), 5 mM PEP, 10 mM $MgCl_2$, 10 mM $NaHCO_3$, 0.15 mM NADH, 2 U MDH (Van der Werf et al. 1997). Citrate synthase (CS): 0.1 M Tris-HCl (pH 8.0), 8 mM acetyl-S-CoA, 10 mM sodium oxaloacetate, 10 mM 5,5′-dithiobis (2-nitrobenzoate) (Parvin 1969). Isocitrate lyase (ICL): 0.1 M potassium phosphate buffer (pH 7.0), 5.0 mM $MgCl_2$, 1.0 mM DTT, 0.3 mM NADH, 5.0 mM isocitrate (Van der Werf et al. 1997). MDH: 0.1 M Tris-HCl (pH 8.8), 0.1 mM sodium malate, 10 mM NAD^+ (Park et al. 1995). Malic enzyme (MEZ): 0.1 M Tris-HCl

(pH 7.8), 5 mM $MgCl_2$, 0.6 mM $NADP^+$, 40 mM malate (Van der Werf et al. 1997). Acetate kinase (ACK): 0.1 M Tris-HCl (pH 7.4), 3 mM $MgCl_2$, 2 mM glucose, 0.5 mM $NADP^+$, 1 U HXK, 1 U G6DPH, 1 mM ADP and 4 mM acetyl phosphate (Lamed and Zeikus 1980). LDH: 300 mM potassium phosphate buffer, 2 mM sodium pyruvate, 0.4 mM NADH (Van der Werf et al. 1997). G6PDH: 0.1 M Tris-HCl (pH 7.5), 2.5 mM $MnCl_2$, 2 mM glucose-6-phosphate (G6P), 1 mM DTT and 1 mM $NADP^+$ (Lamed and Zeikus 1980). 6-Phosphate gluconate dehydrogenase (6PGDH): 0.1 M Tris-HCl (pH 7.5), 2.5 mM $MnCl_2$, 2 mM gluconate-6-phosphate, 1 mM DTT and 1 mM $NADP^+$ (Lamed and Zeikus 1980). Specific Entner-Doudoroff (ED) pathway activity was determined from the combined Edd and Eda reactions in a mixture containing: 5 mM 6-phosphogluconate (6PG), 10 mM $MgSO_4$, and 200 mM Tris-HCl (pH 7.2). The reaction was started by adding 50 μl crude cell extract and was incubated at 30°C for 30 min. After addition of 750 μl 0.2% (w/v) and 2,4-dinitrophenylhydrazine in 500 mM HCl, incubation at room temperature for 10 min, and stopping the reaction by adding 500 μl 4 mM NaOH, the reaction product PYR was detected by recording the extinction at 450 nm. PYR was used as a standard (Canonaco et al. 2001).

Determination of intracellular metabolite concentrations

Cell suspension (10 ml) was rapidly drawn into a syringe and mixed with 30 ml quenching fluid, 60% (v/v) aqueous methanol containing 70 mM HEPES (2-[4-(2-hydroxyethyl)-1-piperazinyl] ethanesulfonic acid) that was kept at −80°C. The cells were separated from the culture by centrifugation for 15 min at 10,000 *g* and 0°C. To extract metabolites from the cell pellet, 500 μl methanol and water mixture was added, and the cells were resuspended by vortexing the mixture. Perchloric acid (2 ml; 35%) was added, and cells were then stored at −80°C after one freeze-thaw cycle; proteins and cell fragments were removed by centrifugation (20,000 *g*; 0°C; 15 min). The clear supernatant was neutralized by adding 895 μl 5 M potassium carbonate solution. Afterward, precipitated perchlorates were removed by another centrifugation step (20,000 *g*; 0°C; 15 min). The clear, neutralized cell extract was stored as 200-μl aliquots at −20°C until further analysis (Buchholz et al. 2001). Enzymatic determination of intracellular metabolites was performed using a fluorescence spectrophotometer (F-4010, Hitachi, Japan). The concentrations of G6P, F6P, 6PG, PEP and PYR were measured according to Schaefer et al. (1999).

Labeling experiments

Isotope labeling experiments were initiated after the culture reached steady state, which was inferred from the stable oxygen and carbon dioxide concentrations in the off-gas and stable OD in the effluent medium for at least twice as long as the residence time. The feed medium with 5 g unlabeled glucose per liter was then replaced by an identical medium containing 0.4 g uniformly labeled glucose [U-^{13}C], 0.4 g of the first carbon labeled glucose [1-^{13}C] and 4.2 g of naturally labeled glucose per liter. Biomass samples for GC-MS/NMR analysis were taken after one residence time.

Sample preparation and analytical procedures for GC-MS analysis

For isotopomer mass analysis of cellular amino acids, 30 ml culture broth was harvested and centrifuged at 12,000 *g* for 10 min at 4°C. The pellet was washed twice with distilled water and centrifuged again. About 20 mg wet biomass was then transferred to 1 ml 6 M HCl. The closed tube was heated for 24 h at 110°C to effect complete hydrolysis and, after cooling to room temperature, the solvent was evaporated with a vacuum dryer. Distilled water (~1 ml) was added to the dried hydrolysates, which was then filtered through a 0.2 μm pore size filter to separate cell debris. The filtrate was dried again and redissolved in 0.5 ml acetonitrile (chromatographic grade) for GC-MS analysis.

For analytical procedures, 100 μl acetonitrile containing biomass hydrolysate was added to 100 μl *N*-(tert-butyldimethylsilyl)-*N*-methyl-trifluroacetamide (TBDMS-FA) (derivatization grade, Aldrich, St. Louis, Mo.). The mixture was incubated for 60 min at 110°C for complete derivatization. After cooling to room temperature, aliquots of the solution containing the derivatives were used directly for GC-MS. GC-MS analysis was carried out using AutoSystem XL GC (Perkin Elmer Biosystems, Foster City, Calif.) equipped with a DB-5MS column (30 m ×0.25 mm ×0.25 μm, Agilent, Fort Collins, Co.), which directly connected to a TurboMass Gold spectrometer (Perkin Elmer). The injection volume was 1 μl with flow mode in split control. The carrier gas flow was set at 1 ml/min. The oven temperature was initially held at 80°C for 2 min. Thereafter, the temperature was raised with a gradient of 8°C/min until the temperature reached 290°C. This temperature was held for 30 min. Other settings were as follows: 250°C interface temperature, 200°C ion source temperature, and electron impact ionization at 70 eV. Mass spectra were analyzed by both full scan mode and selected ion monitoring mode. Raw MS data were processed using the program TurboMass Gold V4.3 (Perkin Elmer) to obtain a purified spectrum by removing residual background contaminants, partially eluting peaks, and column bleed from the spectrum.

Sample preparation and analytical procedure for NMR analysis

At the end of the labeling experiment, culture samples (300 ml) were harvested by centrifugation at 10,000 *g* for 10 min at 4°C. The cell pellet was washed once with 20 mM Tris-HCl (pH 7.6), and hydrolyzed in 6 ml 6 M HCl for 12 h at 105°C. In the resulting hydrolysate, 16 proteinogenic amino acids were present, since cysteine and trytophan were oxidized, while asparagine and glutamine were deaminated during acid hydrolysis. The hydrolysate was filtered through a 0.2 μm pore size filter, and evaporated to dryness. The dried material was dissolved in 700 μl 20 mM deuterium chloride in D_2O, filtered and used for NMR measurements. The labeling patterns of amino acids in the hydrolysates were determined by NMR spectroscopy. The measurements were performed at 30°C and 400 MHz with a Bruker Avance 400 spectrometer (Bruker, Karlsruhe, Germany). Two-dimensional proton-detected ^{1}H–^{13}C heteronuclear multiple-quantum correlation (HMQC) spectra were recorded. For each labeling experiment, two spectra were measured: one focused on aliphatic carbons with the ^{13}C carrier set to 45 ppm, and the other on aromatic rings with the ^{13}C carrier set to 125 ppm. The measurement time of the aliphatic spectra was 15.5 h (data size 3,072×1,024 complex points, t_{1max}=360 ms; t_{2max}=128 ms). Before Fourier transformation, the time domain data were multiplied by t_1 and t_2 with the sine-bell windows shifted by $\pi/2$. The digital resolutions along ω_1 after prediction and zero-filling were 0.86 Hz/point for aliphatic spectra and 1.47 Hz/point for aromatic spectra. All NMR data processing was performed using Bruker XWINNMR software. The cross-section along the ^{13}C axis through the most intense part of each cross peak in the 2D spectra was used for spectrum analysis. After manual baseline correction, the various peaks in the cross-section were integrated to quantify the relative contributions of singlet, doublet, and doublet of doublets signals to the overall multiplet pattern of the carbon signal.

Estimation of metabolic flux distribution

Pools of intracellular metabolites were assumed to be in isotopomeric steady state during the labeling experiments, but such a state was not achieved in the isotopomer distribution of the amino acid and protein pools over the course of the labeling experiment that lasted one volume change in the chemostat. Assuming that the labeling biomass follows first-order wash-out kinetics (Van Winden et al. 2001), the GC-MS data on the amino acid isotopomer composition were corrected for the deviation from the isotopic steady state at the time of harvesting the biomass (Marx et al. 1996;

Szyperski et al. 1999; Möllney et al. 1999) using an isotopic non-steady-state correction based on Van Winden (2001). Also, due to the occurrence of natural isotopes, a correction for GC-MS data was performed by taking into account the contribution of labeling arising from naturally labeled isotopes (^{2}H, ^{13}C, ^{17}O, ^{18}O, ^{15}N, ^{29}Si, ^{30}Si) by a matrix-based method based on the algorithm proposed by Lee (1991).

The isotopomer balance systems were described using isotopomer mapping matrices (Schmidt et al. 1997) and solved through an iterative scheme, based on the approach of Schmidt et al. (1999). The isotopomers of the proteinogenic amino acids were used to generate NMR synthetic patterns.

For the representation of the metabolic fluxes, the forward $v^{\rightarrow}$ and backward $v^{\leftarrow}$ fluxes associated with each bidirectional reaction step were transformed into a net $v^{net} = v^{\rightarrow} - v^{\leftarrow}$, and the exchange flux $v^{exch} = \min(v^{\rightarrow}, v^{\leftarrow})$, which quantifies the amount of flux common to forward and backward fluxes (Wiechert et al. 1997). A non-linear mapping from exchange fluxes to exchange coefficients $v^{exch[0,1]}$ was made to overcome the numerical problems arising from very large parameters values (Schmidt et al. 1999), and because its properties are more suited to linearized statistical analysis (Wiechert and de Graaf 1997) such that:

$$v^{exch[0,1]} = \frac{v^{exch}}{\beta + v^{exch}} \quad (1)$$

where the exchange constant β is usually set equal to the specific glucose uptake rate. In the flux estimation procedure, the exchange coefficients were constrained to be between 0.00 and 0.95 in order to avoid numerical problems.

The stoichiometric model used for metabolic flux analysis includes all reactions of proteinogenic amino acid biosynthesis and primary carbon metabolism. The model of the carbon fates between the intracellular metabolites and proteinogenic amino acids was developed based on that of Szyperski (1995). The central metabolic network of *E. coli* was constructed based on that described in Lehninger (1975), internet database (KEGG 2002) and other literature (Sauer et al. 1999; Emmerling et al. 2002). The model that includes the reactions of the Embden-Meyerhof-Parnas (EMP) and pentose phosphate (PP) pathways, the tricarboxylic acid (TCA) cycle and reversible anaplerotic fluxes from PEP to oxaloacetate (OAA) are given in Table 1. In the case of glucose as the carbon source, the glyoxylate shunt and the ED pathway are usually inactive in the wild type (Walsh and Koshland, 1985), and therefore were not included in the model.

The reactions for PFK and fructose-1,6-bisphosphate aldolase were combined in the reaction ALD, those of enolase, glyceraldehyde-3-phosphate dehydrogenase, phosphoglycerate kinase and mutase in the reaction ENO, those of CS and aconitase in the reaction GLTA, and the reactions of 2-ketoglutarate dehydrogenase, succinyl-CoA synthase, succinate dehydrogenase, fumarate reductase and fumarase in the reaction AKD. The biomass equation was constructed from the overall biomass composition (Neidhardt and Umbarger 1999).

The reactions through ENO and PCK were considered to be bidirectional, where the backward fluxes represent the reactions catalyzed by fructose-1, 6-bisphosphatase and PPC, respectively. Complete scrambling was assumed for the fumarase reaction MDH. The resulting network consisted of 21 reactions and 19 metabolite balances, with a stoichiometric matrix with rank of 19. The oxidative PP pathway (G6PDH) and MEZ were chosen as the net-free fluxes. Additionally, ten exchange-free fluxes were considered.

The free fluxes were obtained by minimizing the error criterion originating from the weighted residuals of the metabolite balances as well as the weighted residuals between the simulated and measured NMR signals (Dauner et al. 2001). The local minima problems of non-linear optimization associated with flux estimation was overcome by incorporating a two-stage optimization strategy (Arauzo-Bravo and Shimizu 2003). The first stage was a global search method to find the region of the best candidate flux set using a genetic algorithm (Goldberg 1989). The second stage involves a local search method inside the region obtained above using a subspace trust region method based on the interior-reflective Newton method (Coleman and Li 1996).

Table 1 The metabolic model.*AcCoA* Acetyl-CoA, *AKG* α-ketoglutarate, *E4P* erythrose-4-phosphate, *F6P* fructose-6-phosphate, *Glc* glucose, *GAP* glyceraldehyde-3-phosphate, *G6P* glucose-6-phosphate, *Mal* malate, *OAA* oxaloacetate, *PEP* phosphoenolpyruvate, *6PG*6-phosphogluconate, *PTS* phosphotransferase system, *PYR* pyruvate, *Rib5P* ribose-5-phosphate, *Ribu5P*ribulose-5-phosphate, *Sed7P* sedoheptulose-7-phosphate, *Xyl5P* xylulose-5-phosphate

Glycolysis			
PTS	Glc + PEP	→	G6P + PYR
PGI	G6p	↔	F6P
ALD	F6p	→	GAP + GAP
ENO	Gap	↔	PEP
PYK	Pep	→	PYR
PDH	Pyr	→	AcCoA + CO_2
Pentose phosphate pathway			
G6PDH	G6p	→	6PG
6PGDH	6 PG	→	Ribu 5P + CO_2
RPI	Ribu5P	↔	Rib5P
RPE	Ribu5P	↔	Xyl5P
TK1	Rib5P + Xyl5P	↔	Sed7P + GAP
TK2	E4P + Xyl5P	↔	F6P + GAP
TAL	Sed7P + GAP	↔	F6P + E4P
Tricarboxylic acid cycle			
GLTA	ACA + OAA	→	Isocitrate
ICD	ICI	↔	AKG + CO_2
AKD	AKG + AKG	→	Mal + CO_2
MDH	Mal	↔	OAA
Glyoxylacetate pathway			
ACE	ICI + AKG	→	SUC + MAL
Anaplerotic pathway			
PPC	Pep + CO_2	↔	OAA
MEZ	Mal	→	PYR + CO_2
Products			
ACK	AcCoA	→	Acetate

Results

Batch culture

Fermentation characteristics

Aerobic cultivation was carried out under controlled conditions in order to assess the *pykF*⁻ gene knock-out in terms of cell growth rate, glucose consumption rate, and metabolite formation rate (Fig. 1). In wild type cultivation, an exponential increase in cell growth was observed during the first 6 h. This is consistent with the rapid increase in CO_2 evolution rate and acetic acid formation, where the maximum acetic acid concentration was 1.187 g/l. The growth rate of the mutant was a little lower compared to that of the wild type. During exponential growth, acetic acid was also produced but its formation rate was significantly lower (maximum concentration 0.403 g/l) compared with that of the wild type. Figure 2 compares the CO_2 evolution rates for the

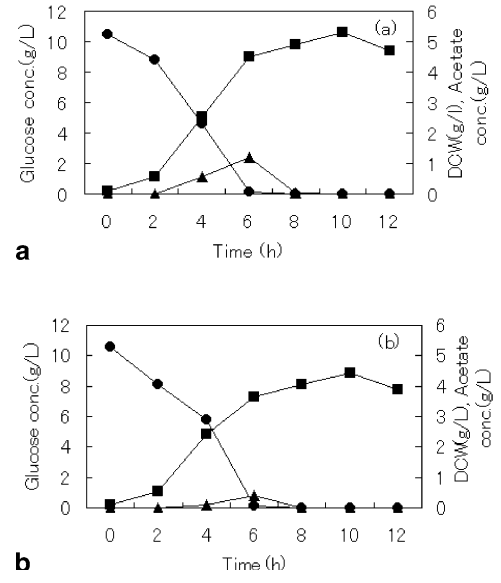

Fig. 1 Batch cultivation of **a** *Escherichia coli* K-12 or **b** *E. coli pyk F*⁻ mutant under aerobic conditions. ● Glucose concentration, ■ biomass concentration, ▲ acetate concentration

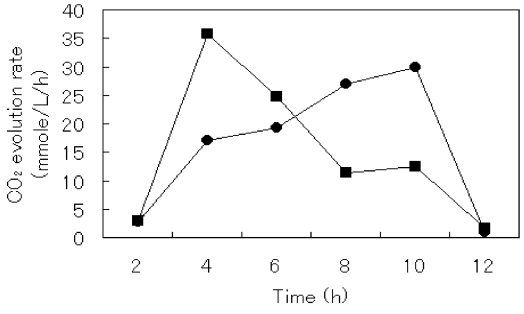

Fig. 2 Comparison of CO_2 evolution rate during batch culture: ■ *E. coli* K 12, ● *E. coli pyk* F⁻ mutant

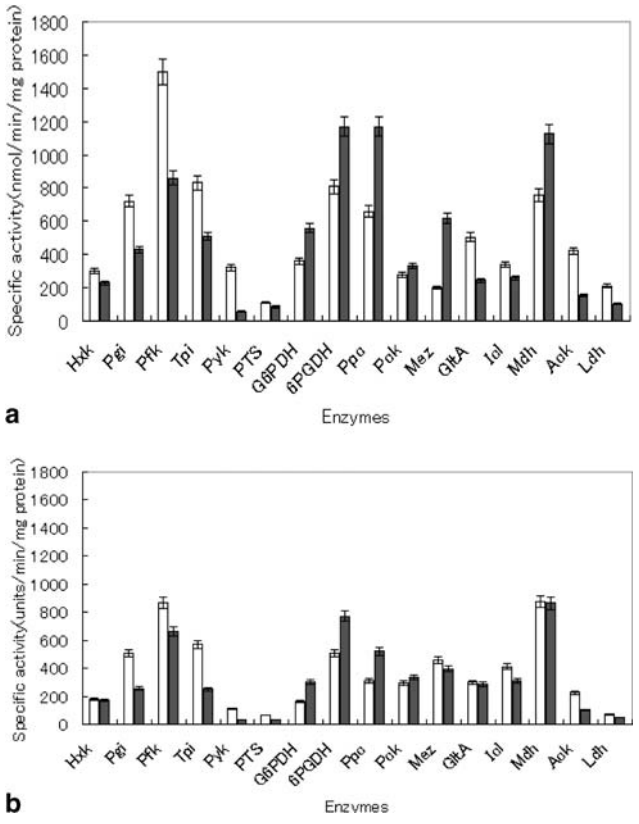

Fig. 3 Comparison of enzyme activities during 4 h (**a**) or 8 h (**b**) of batch culture. □ E. coli K-12, ■ *E. coli pyk F*⁻ mutant. *Hxk* Hexokinase, *Pgi* phosphoglucose isomerase, *Pfk* phosphofructose kinase, *Tpi* triosephosphate isomerase, *Pyk* pyruvate kinase, *PTS* phophoglucose transferase, *G6PDH* glucose-6-phosphate dehydrogenase, *6 PGDH* 6-phosphogluconate dehydrogenase, *Ppc* phosphoenol pyruvate carboxylase, *Pck* phosphoenol pyruvate carboxykinase, *Mez* malic enzyme, *GltA* citrate synthase, *Icl* isocitrate lyase, *Mdh* malate dehydrogenase, *Ack* acetate kinase *Ldh* lactate dehydrogenase

two strains: the CO_2 evolution rate was lower for the *pykF*⁻ mutant during the initial 6 h compared to that of the wild type. The decrease in CO_2 evolution rate in the *pykF*⁻ mutant might be partly due to an increase in CO_2 fixation through the PPC enzymatic reaction as will be explained later in this paper. Another possibility may be decreased glucose consumption rate.

Glycolytic pathway enzymes

Various enzymes play significant roles in the control of catabolic flux in *E. coli* depending on the strain and culture conditions. Several enzyme activities for glycolytic enzymes (HXK, PGI, PFK, TPI and PYK) were measured for both the wild type and *pykF*⁻ mutant of *E. coli*. The enzyme activity of the PEP:phosphoglucose transferase system (PTS) was detected only in the presence of glucose (Fig. 3a), confirming its efficient induction by glucose. HXK activity also increased when glucose was present. This enzyme is thought to be inhibited by its product G6P. High activities of other glycolytic enzymes (PGI, TPI and PYK) during 2–6 h of fermentation indicate a "stepping up" of glucose utilization during fermentation. All these enzymes are under control of catabolic repression/activation mechanisms. All the enzyme activities mentioned were repressed under acetate conditions as compared to the case when glucose was present. When the acetate was fully consumed, these activities recover from the repression as shown in Fig. 3b. The enzyme activity of PYK was significantly lower in the *pykF*⁻ mutant as compared with that of wild type K-12 during the whole period of fermentation, confirming deletion of the *pykF* gene in the mutant.

Anaplerotic and oxidative PP pathway enzymes

The anaplerotic enzyme PPC is usually active when glucose is present as well as during the exponential growth phase to supply OAA for the production of

biosynthetic compounds. This enzyme activity was found to be higher during the first 4 h of fermentation in both wild type and the *pykF*⁻ mutant when glucose was present. Moreover, compared with that of the wild type, an increased activity was found in the *pykF*⁻ mutant during 2–4 h of fermentation. As acetate was formed, the activity of the gluconeogenic enzyme PCK became higher compared to the case where only glucose was present. Moreover, it can also be seen that a higher activity of PCK was observed for the *pykF*⁻ mutant as compared with that of *E. coli* K12 (see Fig. 3a, b).

The oxidative PP pathway enzymes G6PDH and 6 PGDH seem to be under acetate repression like other glycolytic enzymes. But these enzyme activities were higher in the *pykF*⁻ mutant than in the wild type (Fig. 3a), in particular when glucose was present.

Other enzymes and TCA cycle enzymes

The enzyme activity of MEZ is usually very low in bacteria when glucose is present. But this enzyme activity increased 3-fold in the *pykF*⁻ mutant compared to the wild-type strain in the presence of glucose. This high activity might be due to the high activity of pyruvate carboxylase. The activity of this enzyme was found to be higher when acetate was utilized as a carbon source in the wild type (Fig. 3a, b). MDH activity was also increased in the *pykF*⁻ mutant, showing a trend similar to that of MEZ (Fig. 3a, b)

Citrate synthase (encoded by *glt*A), the entry enzyme to TCA cycle, was found to be suppressed by excess glucose, but elevated by oxygen and other carbon sources such as acetate. During the first 2 h, this enzyme was not very active, but it became more active upon glucose-acetete co-metabolism conditions. As compared with the *pykF*⁻ mutant, this enzyme activity was higher in the wild type. The glyoxalate shunt enzyme, ICL, encoded by the gene *ace*A is usually activated by acetic acid to supply the OAA needed for anaplerosis. Thus, this enzyme activity was found to be higher when acetate was utilized as a carbon source. Other enzymes such as ACK and LDH were also measured for both strains. These enzyme activities were found to be higher in the presence of glucose. ACK and LDH activities were found to be lower in the *pykF*⁻ mutant than in the wild type (Fig. 3a). Enzyme activities of the ED pathway could not be detected in the present study under either glucose or acetate conditions.

Intracellular metabolite concentrations

Intracellular metabolite concentrations are also quite important when investigating metabolic regulation. We therefore determined the intracellular concentrations of glycolytic and oxidative PP pathway intermediates. The metabolites measured included G6P, F6P, gluconate-6-phosphate, PEP and PYR. The time courses of the change

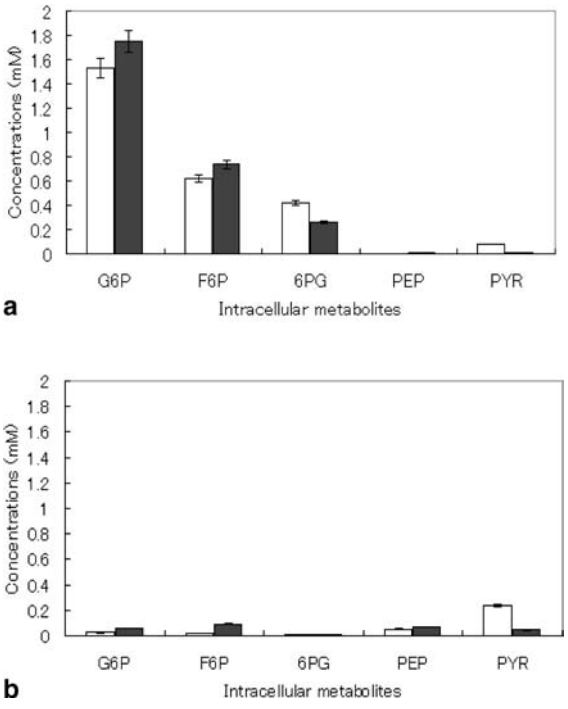

Fig. 4 Intracellular metabolite concentrations during 4 h (**a**) or 8 h (**b**) of batch cultivation. □ *E. coli* K-12, ■ *E. coli pykF*⁻ mutant. *G6P* Glucose-6-phosphate, *F6P* fructose-6-phosphate, *6PG* gluconate-6-phosphate, *PEP* phosphoenol pyruvate, *PYR* pyruvate

Table 2 Growth parameters of of *Escherichia coli* mutant *pykF*⁻ at two different dilution rates (*D*)

Growth parameters	*pykF*⁻ mutant grown at	
	D =0.1 h^{-1}	D =0.5 h^{-1}
Biomass yield (g g^{-1})	0.481	0.42
Glucose uptake rate (mmol g^{-1} h^{-1})	1.81	6.94
CO_2evolution rate (mmol g^{-1} h^{-1})	3.7	16.8

in those metabolite concentrations are shown in Fig. 4a, b; the PYR concentration was lower and the PEP concentration slightly higher in than the *pykF*⁻ mutant as compared with the values in *E. coli* K12. It can also be seen that G6P and F6P concentrations were higher in the *pykF*⁻ mutant of *E. coli* as compared with those of wild type.

Continuous culture

Continuous cultivation was conducted at two different dilution rates (D=0.1 h^{-1} and 0.5 h^{-1}). The growth parameters of the *E. coli pykF*⁻ mutant are summarized in Table 2. The glucose uptake and carbon dioxide evolution rate were both high at the higher D value.

To obtain higher resolution on the intracellular isotope distribution, we used both GC-MS and NMR. Möllney et al. (1999) indicated that mass isotopomer analysis using a mixture of uniformly labeled glucose and naturally

Table 3 Fragment mass distribution of t-butyldimethylsilyl (TBDMS)-derivatized amino acids from the *pykF*⁻ mutant. Considering standard deviation in the range 0.002 to 0.006 for mass distribution, only mass signals of *m*, *m*+1 and *m*+2 were compared. *Asx*, *Glx* Asparagine and glutamine deaminated during acid hydrolysis

Amino acids	Fragments	*m*	*m*+1	*m*+2
Ala	$[M-57]^+$	0.699[a]	0.181	0.099
		0.693[b]	0.180	0.097
Asx	$[M-57]^+$	0.650[a]	0.250	0.078
		0.666[b]	0.043	0.031
Gly	$[M-57]^+$	0.744[a]	0.160	0.096
		0.735[b]	0.156	0.093
Glx	$[M-57]^+$	0.540[a]	0.170	0.162
		0.539[b]	0.167	0.153
Ile	$[M-57]^+$	0.685[a]	0.079	0.085
		0.681[b]	0.075	0.080
Ile	$[M-159]^+$	0.641[a]	0.079	0.071
		0.639[b]	0.077	0.084
Leu	$[M-57]^+$	0.677[a]	0.129	0.084
		0.671[b]	0.126	0.081
Leu	$[M-57]^+$	0.614[a]	0.112	0.112
		0.610[b]	0.102	0.106
Phe	$[M-57]^+$	0.629[a]	0.116	0.110
		0.627[b]	0.113	0.097
Phe	$[M-159]^+$	0.568[a]	0.112	0.077
		0.565[b]	0.110	0.075
Met	$[M-57]^+$	0.608[a]	0.041	0.029
		0.606[b]	0.039	0.028
Thr	$[M-57]^+$	0.587[a]	0.242	0.133
		0.586[b]	0.238	0.127
Tyr	$[M-57]^+$	0.617[a]	0.115	0.099
		0.616[b]	0.111	0.095
Tyr	$[M-159]^+$	0.544[a]	0.108	0.076
		0.543[b]	0.106	0.072
Val	$[M-57]^+$	0.640[a]	0.081	0.067
		0.642[b]	0.078	0.063

[a] Experimentally determined
[b] Calculated

Table 4 Measured and simulated values of the 2D heteronuclear multiple-quantum correlation (HMQC) NMR spectra of cellular amino acids. *s* Singlet, d_1 doublet with larger scalar coupling, d_2 doublet with smaller scalar coupling, *dd* doublet of doublets

Atom	Measured				Simulated			
	s	d_1	d_2	dd	s	d_1	d_2	dd
Arg γ	0.39	0.61	–	–	0.35	0.63	–	–
Asx α	0.39	0.61	–	–	0.38	0.52	–	–
Gly α	0.34	0.66	–	–	0.32	0.60		
Ile α	0.19	0.11	0.61	0.09	0.17	0.01	0.62	0.02
Ile δ	0.35	0.65	–	–	0.30	0.56	–	–
Leu α	0.17	0.08	0.66	0.09	0.12	0.01	0.63	0.02
Leu β	0.43	0.57	–	0.00	0.42	0.56	–	0.00
Lys ε	0.32	0.68	–	–	0.34	0.63	–	–
Pro α	0.11	0.15	0.19	0.55	0.08	0.12	0.14	0.55

labeled glucose yielded poor results. Therefore, we used a mixture of uniformly labeled [U-^{13}C] glucose, first carbon labeled [1-^{13}C] glucose and naturally labeled glucose in the present study. The GC-MS and NMR data for the *E. coli pykF*⁻ mutant are shown in Tables 3 and 4, while those for wild type can be found elsewhere (Yang et al. 2003). Figure 5 shows the intracellular flux distributions determined for wild type (upper figures) and for the *pykF*⁻ mutant (lower figures). The flux distribution in the *pykF*⁻ mutant reveals a high flux from PEP to OAA. The flux through the anaplerotic reaction catalyzed by PPC in the *pykF*⁻ mutant was also high (at 44%) in the *pykF*⁻ mutant as compared with 17% for the wild-type strain. It should be noted that the flux value in brackets in Fig. 5 for PPC is also high, which indicates that the flux through PCK is also high. The flux from PEP to PYR was 1.6% for the *pykF*⁻ mutant, which is significantly lower compared to 130% for wild type and is consistent with the enzyme activity measurement. It can also be seen that the flux though MEZ is high, about 21% for the *pykF*⁻ mutant, while it is very low (~3%) for wild type. Moreover, the glycolytic flux from G6P to F6P was 20% for the *pykF*⁻ mutant, while it was 65% in the wild-type strain. Note that we lumped the PGI and PFK reactions together for flux calculation. On the other hand, flux through the oxidative PP pathway was 79% for *pykF*⁻ mutant, while it was 34% in the wild type. The flux from acetylCoA to acetate reduced to 0.82% in the *pykF*⁻ mutant as compared with 20% in the wild type.

Some of the enzyme activities and intracellular metabolite concentrations for the central metabolic pathways of the *pykF*⁻ mutant of *E. coli* were also measured for continuous culture at two different dilution rates. The results are shown in Figs. 6 and 7. The enzyme activities for glycolytic pathway enzymes such as HXK, PGI and TPI decreased by about 2.65-,2.45-, and 2.08-fold at high *D* (0.5 h^{-1}) compared with those at low *D* (0.1 h^{-1}). Figure 6 shows that the enzyme activity of PFK decreased slightly as *D* increased, which may be due to the increase in the intracellular concentration of PEP as shown in Fig. 7. The decreased activity of PFK at high *D* increased the concentrations of G6P and F6P, which in turn increased the enzyme activities of G6PDH and 6 PGDH, by about 3- and 9-fold, respectively. The enzyme activity of PYK at both *D* values was very low. The enzyme activity of MEZ decreased by about 3.5-fold at high *D*. In accordance with this phenomenon, PCK activity decreased at high *D*. The enzyme activity of the TCA cycle enzyme GLTA was lower at high *D*, while that of MDH changed little at both *D* values. The enzyme activity of the ED pathway was found to be higher at high *D*. This corresponds to the increase in carbon flow in the oxidative PP pathway. LDH activity was also increased 2.25-fold at high *D*. This might be due to the increased activity of the ED pathway at high *D*. Although the LDH reaction requires NADH, it is not produced through the ED pathway. Therefore, NADPH produced through the oxidative PP pathway might have been utilized for this reaction. The enzyme activities of ACK and isocitrate dehydrogenase were also measured for both *D* values, but found to be little changed.

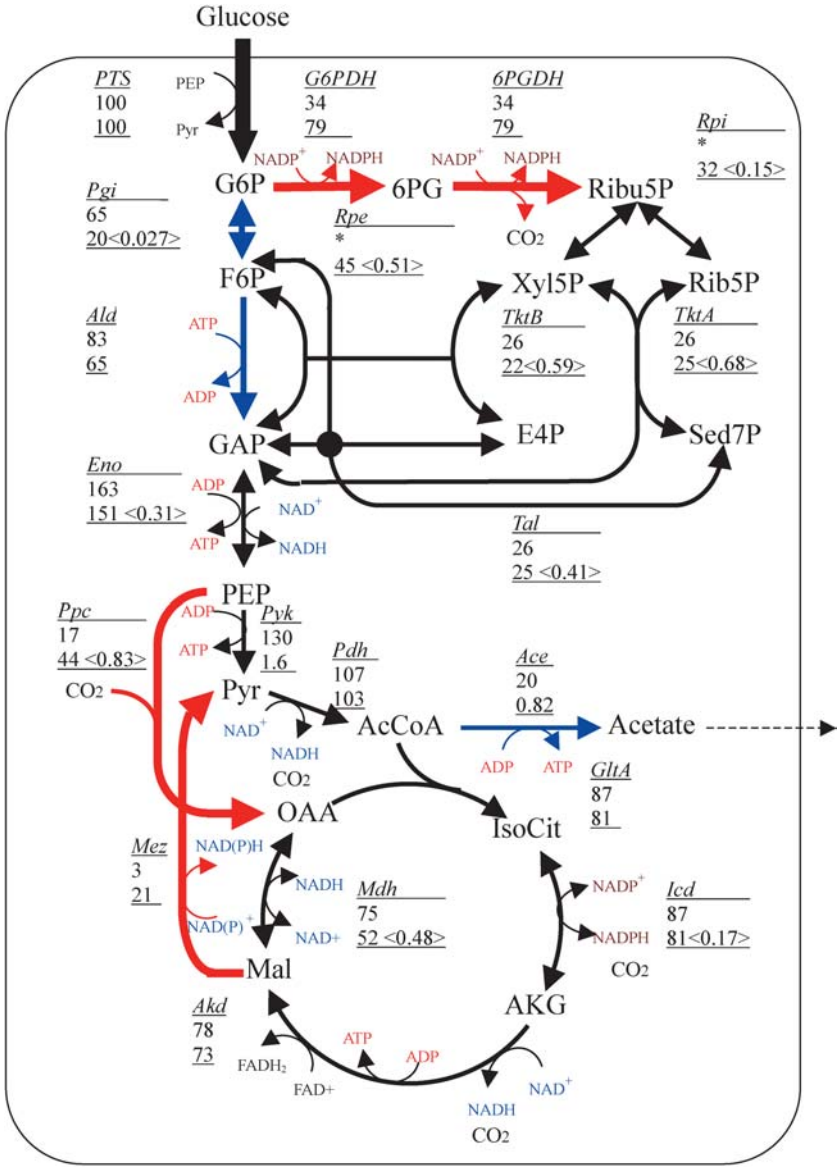

Fig. 5 Metabolic flux distribution of wild type (upper value) and *pykF*$^{-}$ mutant (lower value) at dilution rate (D) of 0.1 h^{-1}. The deep red color indicates increased flux and blue color indicates reduced flux for *pyk F*$^{-}$ mutant. Values in < > indicate exchange coefficient. *AcCoA* Acetyl-CoA, *AKG* α-ketoglutarate, *Asp* aspartate, *E4P* erythrose-4-phosphate, *F6P* fructose-6-phosphate, *FBP* fructose-1,6-bisphosphate, *Glc* glucose, *Glu* glutamate, *GAP* glyceraldehyde-3-phosphate, *G6P* glucose-6-phosphate, IsoCit isocitrate, *Mal* malate, *OAA* oxaloacetate, *PEP* phosphoenolpyruvate, *6PG* 6-phosphogluconate, *PP* pentose phosphate, *PTS* phosphotransferase system, *PYR* pyruvate, *Rib5P* ribose-5-phosphate, *Ribu5P* ribulose-5-phosphate, *Sed7P* sedoheptulose-7-phosphate, *Xyl5P* xylulose-5-phosphate

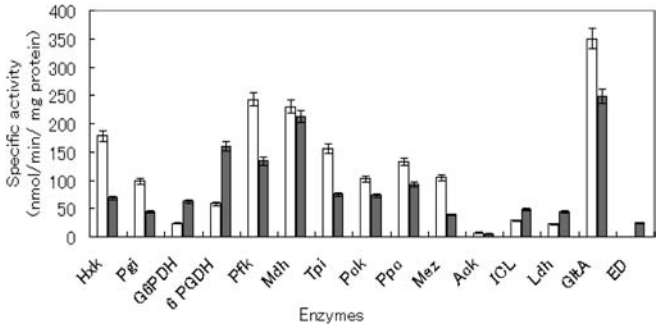

Fig. 6 Enzyme activities for the *pyk F*$^{-}$ mutant at two D values: □ 0.1 h^{-1}, ■ 0.5 h^{-1}. *ED* Entner-Doudoroff pathway, other abbreviations are as in Fig. 3

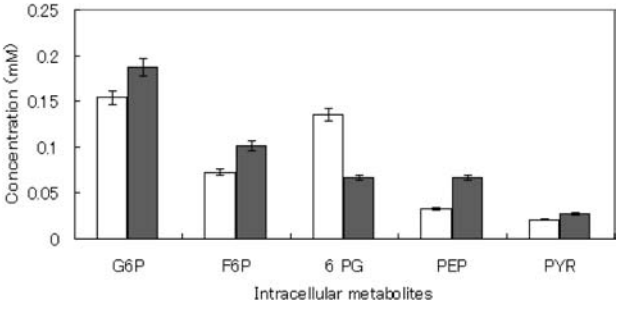

Fig. 7 Comparison of concentrations of intracellular metabolites in the *pykF*$^{-}$ mutant at two D values: □ 0.1 h^{-1}, ■ 0.5 h^{-1}. Abbreviations are as in Fig. 4

Discussion

The primary objective of the present study was the quantitative elucidation of metabolic regulation in response to *pyk* knockout in *E. coli*. In the present study, we first performed a batch cultivation using both wild type *E. coli* K-12 and a *pyk F*$^-$ mutant to gain deeper insight into the physiological changes with respect to enzyme activities and intracellular metabolite concentrations. In batch culture, it was found that the *pykF* gene knockout has little effect on cell growth. However, acetate production was substantially lower for the *pykF*$^-$ mutant compared to wild type. These results are consistent with other researches made by Ponce et al. (1998) and Zhu et al. (2001). In the present study, it was found that the enzyme activities of glycolytic enzymes such as HXK, PGI, PFK, TPI and PPC were higher during 2–4 h of fermentation as shown in Fig. 3. When glucose was depleted, these enzyme activities were downregulated. As soon as the acetate was consumed, these enzymes were derepressed, and their activities increased again from 8 to 12 h of fermentation (Fig. 3b). These results correspond to those observed by Oh et al. (2002), where they showed by DNA microarray analysis that, during acetate metabolism, glycolytic genes such as *pfk*, *fba*, *ppc*, *pyk*, *zwf* and *gnd* were downregulated. These genes are thought to be regulated by the catabolite repressor/activator *cra*, a global catabolite repression regulator (Saier and Ramseier 1996). Early investigation showed that glucose transport genes exhibit high basal expression, and the *ptsH* gene is positively stimulated by cAMP-CRP receptor protein during growth on glucose, while *crr* promoters within the *pts1* operon may be negatively regulated by CRP-cAMP (Reuse and Danchin 1988; Fox et al. 1992). Plumbridge (1999) reported that these genes are in the same operon, which is known to be regulated by *Mlc* in the absence of glucose, with *Mlc* repressing the operon. For this reason, a low activity of PTS was observed during growth on acetate as a carbon source. The gluconeogenic enzyme PCK is known to be responsible for delivering the carbon flux from the TCA cycle to the gluconeogenic pathway during acetate metabolism. This was observed in our study; during 4 h of fermentation, the activity of this enzyme activity tended to increase, showing full activation when acetate was used as carbon source. The *pck*A gene may be induced by the increased level of cAMP. This type of trend was also observed for MEZ. Oh et al. (2002) found in their study that MEZ and PCK enzyme correlated when acetate was utilized. They explained that the mutation of *mez* and *pck*A genes prevented growth on acetate. As the glucose is consumed and acetate accumulates, cells switch smoothly to cometabolism, utilizing both glucose and acetate. This switch involves induction of the TCA cycle enzymes and glyoxalate bypass enzymes required to provide energy and to replenish intermediates used for amino acid biosynthesis (Clark and Cronan 1996). We observed similar phenomena in the case of GLTA, which was more active when both glucose and acetate were utilized during 4–6 h of fermentation (Fig. 3a). ICL also became more active under acetate conditions (Fig. 3b). TCA cycle genes are known to be under the control of cAMP and CRP, which mediate catabolic repression (Cronan and LaPorte 1999). *E. coli* satisfies energy requirements through glycolysis by producing large amounts of NADH, where the NADH produced must be reoxidized to NAD^+, which is required to maintain glycolysis since it is again the substrate for glyceraldehyde-3-phosphate dehydrogenase in glycolysis. Therefore, the activity of LDH increased on glucose as carbon source and was repressed under acetate conditions (Fig. 3a, b). ACK was also found to be active under glucose conditions and repressed under acetate conditions.

We also studied how changes in enzymatic activity affect intracellular metabolite concentrations. We found that when extracellular glucose was present, the intracellular concentrations of glycolytic intermediates and oxidative PP pathway intermediates such as G6P, F6P and 6PG were higher (Fig. 4a). As a result of higher enzyme activity, the concentrations of these intracellular metabolites were reduced after 4 h of growth. The PEP concentration was found to be not so high during the first 4 h of fermentation, which indicates that most of the PEP may be utilized in the glucose transport system.

In the case of the *pykF*$^-$ mutant, it was found that the enzyme activities of glycolytic pathway enzymes decreased as compared with those of wild type, while the enzyme activities of oxidative PP pathway enzymes increased for the former. Ponce et al. (1998) also reported increased activities of oxidative PP pathway enzymes in the *pykF*$^-$ mutant. The most significant differences between wild type and *pyk F*$^-$ mutant were observed in PPC and MEZ activities. In the presence of glucose, these two enzyme activities were significantly increased in the *pykF*$^-$ mutant. This can be explained by the fact that the blockage of PEP to PYR pathway activated both PPC and MEZ enzymes to supply PYR by forming an alternative pathway. It was thought that blockage of PEP to PYR would increase the PEP pool in the mutant, which might inhibit PFK enzyme activity in the glycolytic pathway. A slight increase in the PEP pool was observed for the *pykF*$^-$ mutant at 4 h of fermentation. The decreased activity of PFK in turn increased the G6P and F6P concentrations. Increased activity of the oxidative PP pathway was observed in the *pykF*$^-$ mutant. This might be due to the increased G6P concentration. Over produced NADPH in the PP pathway may be partly utilized through LDH reaction in the *pykF*$^-$ mutant.

From the investigation on continuous culture, the flux calculation result shows clearly that disruption of PYK increases the flux through PPC and MEZ. The flux result also shows reduced carbon flow through glycolysis and increased carbon flow through the PP pathway, which is consistent with the measurements of enzyme activities and intracellular metabolite concentrations. A higher flux through the anaplerotic pathway was obtained for the *pykF*$^-$ mutant. This may lead to ATP dissipation since PCK constitutes a futile cycle during growth on glucose in

the *pykF*⁻ mutant. Although futile cycling could be induced by simultaneous overexpression of *Ppc* and *Pck* in *E. coli* (Chao and Laio 1994), it is generally maintained at a low level (Chambost and Fraenkel 1980; Dalal and Fraenkel 1983; Chao and Laio 1994). The enzyme activity results for PPC and PCK support the futile cycle result obtained by flux calculation since, in batch culture, these two enzyme activities were also found to be higher in the *pykF*⁻ mutant compared to the wild type K-12.

Comparison of the results at two dilution rates for the *pykF*⁻ mutant was revealed that the activities of glycolytic pathway enzymes, TCA cycle enzymes and MEZ became lower at high *D* as compared with those at low *D*, whereas the oxidative PP pathway enzymes were more active at high *D*. ED pathway enzymes, which were usually inactive in the presence of glucose, showed significant activity at high *D*. At high *D*, cells try to grow rapidly, and require PYR etc. for production of biosynthetic compounds. A blockage in the PEP to PYR flow might have induced the mutant to utilize the ED pathway to meet the PYR requirement. For this reason, LDH activity also increased in the *pykF*⁻ mutant at high *D*.

It should be noted that, in the wild-type strain, a change in *D* has the opposite effect compared to the *pykF*⁻ mutant. In the wild-type strain, the enzyme activities of PPC, PCK and TCA cycle enzymes increased at high *D* as compared with those at low *D*. Also, the intracellular PEP concentration was low at high *D* as compared with that at low *D*.

In conclusion, combining results of enzyme activities, intracellular metabolite concentrations, and information on metabolic flux distribution obtained based on ^{13}C-labelling experiments, can be quite useful in uncovering metabolic regulation caused by gene knock-out or changes in culture conditions.

Acknowledgement It is acknowledged that this research was supported in part by a grant from New Energy and Industrial Technology Development Organization of Japan (NEDO) of the Ministry of Economy, Trade and Industry of Japan (Development of a Technological Infrastructure for Industrial Bioprocess Project).

References

Arauzo-Bravo MJ, Shimizu K (2003) An improved method for statistical analysis of metabolic flux analysis using isotopomer mapping matrices with analytical expressions. J Biotechnol (in press)

Buchholz A, Takors R, Wandrey C (2001) Quantification of intracellular metabolites in *Escherichia coli* K-12 using liquid chromatographic-electron spray ionization tandem mass spectrometric technique. Anal Biochem 295:129–137

Canonaco F, Hess TA, Heri S, Wang TT (2001) Metabolic flux response to phosphoglucose isomerse knock-out in *Escherichia coli* and impact of overall response of the soluble transhydrogenase UdhA. FEMS Microbiol Lett 204:247–252

Chambost JP, Fraenkel DG (1980) The use of 6-labeled glucose to assess futile cycling in *Escherichia coli*. J Biol Chem 255:2867–2869

Chao YP, Laio JC (1994) Metabolic responses to substrate futile cycling in *Escherichia coli*. J Biol Chem 269:5122–5126

Clark DP, Cronan JE (1996) Two-carbon compounds and fatty acids as carbon sources. In: Neidhardt FC et al (eds) *Escherichia coli* and *Salmonella typhimurium*: cellular and molecular biology, 2nd edn. ASM Press, Washington, D.C., pp 343–357

Coleman TF, Li Y, (1996) An interior, trust region approach for nonlinear minimization subject to bounds. SIAM J Optim 6:418–445

Cronan JE Jr, LaPorte D (1999) Tricarboxylic acid cycle and glyoxalate bypass. In: Neidhardt FC et al (eds) *Escherichia coli* and *Salmonella typhimurium*: molecular biology, 2nd edn. ASM press, Washington D.C., pp 343–357

Dalal F, Fraenkel DG (1983) Assessment of a futile cycle involving reconversion of fructose-6-phosphate to fructose-1,6-biphosphate during gluconeogenic growth of *Escherichia coli.* J Bacteriol 153:390–394

Datsenko KA, Wanner BL (2000) One step inactivation of chromosomal genes in *Escherichia coli* K-12 using PCR product. Proc Natl Acad Sci USA 97:6640–6645

Dauner M, Bailey J, Sauer U (2001) Metabolic flux analysis with a comprehensive isotopomer model in *Bacillus subtilis*. Biotechnol Bioeng 76:132–143

Emmerling M, Dauner M, Aaron P, Fiaux J, Hochuli M, Szyperski T, Wüthrich K, Bailey JE, Sauer U (2002) J Bacteriol 184:152–164

Fraenkel DG (1992) Genetics and intermediary metabolism. Annu Rev Genet 26:159–177

Fox DK, Presper KA, Adhya S, Roseman S, Ganges S (1992) Evidence of two promoters upstream of the *pts* operon: regulation by the cAMP receptor protein regulatory complex. Proc Natl Acad Sci USA 89:7056–7059

Gancedo JA, Gancedo C (1971) Fructose-1,6-diphosphatase, phosphofructokinase and glucose-6-phosphate dehydrogenase from fermenting and non fermenting yeasts. Arch Microbiol 76:132–138

Goldberg DE (1989) Genetic algorithms in search, optimization, and machine learning. Addison-Wesley, Reading, Mass.

KEGG (2002) Kyoto encyclopedia of genes and genomes. http://www.genome.ad.jp/kegg

Lamed R, Zeikus JG (1980) Glucose fermentation pathway of *Thermonaerobium brockii*. J Bacteriol 141:1252–1257

Lee PWN (1991) Mass isotopomer analysis: theoretical and practical considerations. Biol Mass Spectrom 20:451–458

Lehninger AL (1975) Biochemistry: the molecular basis of cell structure and function, 2nd edn. Worth, N.Y.

Marx A, De Graaf AA, Wiechert W, Eggeling L, Sahm H (1996) Determination of the fluxes in the central metabolism of *Corynebacterium glutamicum* by nuclear magnetic resonance spectroscopy combined with metabolic balancing. Biotechnol Bioeng 49:111–129

Möllney M, Wiechert W, Kowantzki D, de Graaf AA (1999) Bidirectional reaction steps in metabolic networks. IV Optimal design of isotopomer labeling experiments. Biotechnol Bioeng 66:86–103

Neidhardt FC, Umbarger HE (1999) Chemical composition of *Escherichia coli*. In: Neidhardt FC et al (eds) *Escherichia coli and Salmonella typhimurium*: cellular and molecular biology, 2nd edn. ASM Press, Washington D.C.

Oh MK, Rohlon L, Kao K, Liao JC (2002) Global expression profiling of acetate-grown *E. coli*. J Biol Chem 277:13175–13183

Park SJ, Cotter PA, Gunsalus RP (1995a) Regulation of malate dehydrogenase (*mdh*) gene expression in *Escherichia coli* in response to oxygen, carbon and heme availability. J Bacteriol 177:6652–6656

Parvin R (1969) Citrate synthase from rat liver. Methods Enzymol 13:16–19

Plumbridge J (1999) Expression of the phosphotransferase system both mediates and is mediated by *Mlc* regulation in *Escherichia coli*. Mol Microbiol 33:260–273

Ponce E, Flores N, Martinez A, Bolivar F, Valle F (1995) Cloning of the two pyruvate kinase isoenzyme structural genes from

Escherichia coli: the relative role of these enzymes in pyruvate biosynthesis. J Bacteriol 177:5719–5722

Ponce E, Martinez A, Bolivar F, Valle F (1998) Stimulation of glucose catabolism through the pentose pathway by the absence of the two pyruvate kinase isoenzymes in *Escherichia coli*. Biotechnol Bioeng 58:292–295

Reuse HD, Danchin A (1988) The *ptsH*, *ptsI*, and *crr* genes of the *Escherichia coli* phosphoenol pyruvate-dependent phosphotransferase system: a complex operon with several modes of transcription. J Bacteriol 170:3827–3837

Saier MH, Ramseier TM (1996) The catabolic repressor/activator (*cra*) protein of enteric bacteria. J Bacteriol 178:341–347

Salas M, Vinuela E, Sols A (1965) Spontaneous and enzymatic anomerization of glucose-6-phosphate and anomeric specificity of related enzymes. J Biol Chem 240:561–568

Samuelov NS, Lamed R, Lowe S, Zeikus JG (1991) Influence of CO_2-HCO_3- levels and pH on growth, succinate production and enzyme activities of *Anaerbiospirillum succiniciproducens*. Appl Environ Microbiol 57:3013–3019

Sauer U, Lasko DR, Flaux JL, Hochuli M, Glaser R, Szyperski T, Wüthrich K, Bailey JE (1999) Metabolic flux ratio analysis of genetic and environmental modulations of *Escherichia coli* central carbon metabolism. J Bacteriol 181:6679–6688

Schaefer U, Boos W, Takors R, Weuster-Botz D (1999) Automated sampling device for monitoring intracellular metabolite dynamics. Anal Biochem 270:88–96

Schmidt K, Carlsen M, Nielsen J, Villadsen J (1997) Modeling isotopomer distributions in biochemical networks using isotopomer mapping matrices. Biotechnol Bioeng 55:831–840

Schmidt K, Nielsen J, Villadsen J (1999) Quantitative analysis of metabolic fluxes in *Escherichia coli* using two-dimensional NMR spectroscopy and complete isotopomer models. J Biotechnol 71:175–190

Sridhar J, Eiteman M, Wiegel JW (2000) Elucidation of enzymes in fermentation pathways used by *Clostridium thermosuccino* genes growing on inulin. J Appl Environ Microbiol 66:246–251

Steiner P, Fussenegger M, Bailey JE, Sauer U (1998) Cloning expression of the *Zymomonas mibilis* pyruvate kinase gene in *Escherichia coli.* Gene 220:31–38

Szyperski T (1995) Biosynthetically directed fractional ^{13}C-labeling of proteinogenic amino acid. Eur J Biochem 232:443–448

Szyperski T, Glaser RW, Hochuli M, Fiaux J, Sauer U, Bailey JE, Wüthrich K (1999) Bioreaction network topology and metabolic flux ratio analysis by biosynthetic fractional ^{13}C labeling and two-dimensional NMR spectroscopy. Metabol Eng 1:189–197

Tao H, Bausch C, Richmond C, Blatner RF, Conway T, (1999) Functional genomics: expression analysis of *Escherichia coli* growing on minimal and rich media. J Bacteriol 181:6425–6440

Van der Werf MJ, Guettle MV, Jain MK, Zeikus JG (1997) Environmental and physiological factors affecting the succinate product ratio during carbohydrate fermentation by *Actinobacillus* sp. 130Z. Arch Microbiol 147:195–200

Van Winden W, Schipper D, Verheijen P, Heijnen J (2001) Innovations in generation and analysis of 2D [^{13}C, ^{1}H] COSY NMR spectra for metabolic flux analysis purposes. Metabol Eng 3:322–343

Walsh K, Koshland DE (1985) Branch point control by the phosphorylation state of isocitrate dehydrogenase. J Biol Chem 260:8430–8437

Wiechert W, de Graaf AA (1997) Bidirectional reaction steps in metabolic networks: I. Modeling and simulation of carbon isotope labeling experiments. Biotechnol Bioeng 55:101–117

Wiechert W, Siefke C, de Graff AA, Marx A (1997) Bidirectional reaction steps in metabolic networks: II. Flux estimation and statistical analysis. Biotechnol Bioeng 55:118–135

Yang C, Hua Q, Shimizu K (2003) Analysis of *E. coli* anaplerotic metabolism and its regulation mechanisms from the metabolic responses to altered dilution rates and ppc knockout. Meas Biotechnol Bioeng (in press)

Zhu T, Phalakornkule C, Koepsel RR, Domach MM, Ataai MM (2001) Cell growth and by product formation in pyruvate kinase mutant of *E. coli*. Biotechnol Prog 17:624–628